

# Communities in *C.elegans* connectome through the prism of non-backtracking walks

Arsenii A. Onuchin<sup>1</sup>, Alina V. Chernizova<sup>2</sup>, Mikhail A. Lebedev<sup>3</sup>, Kirill E. Polovnikov<sup>3</sup>

<sup>1</sup>*Lomonosov Moscow State University, 119991 Moscow, Russia*

<sup>2</sup>*Saint Petersburg State University, 198504 Saint Petersburg, Russia*

<sup>3</sup>*Skolkovo Institute of Science and Technology, 121205 Moscow, Russia*

The fundamental relationship between the mesoscopic structure of neuronal circuits and organismic functions they subserve is one of the major challenges in contemporary Neuroscience. Formation of structurally connected modules of neurons enacts the conversion from single-cell firing to large-scale behaviour of an organism, highlighting the importance of their accurate profiling in the data. While connectomes are typically characterized by significant sparsity of neuronal connections, recent advances in network theory and machine learning have revealed fundamental limitations of traditionally used community detection approaches in cases where the network is sparse. Here we studied the optimal community structure in the structural connectome of *C.elegans*, for which we exploited a non-conventional approach that is based on non-backtracking random walks, virtually eliminating the sparsity issue. In full agreement with the previous asymptotic results, we demonstrated that non-backtracking walks resolve the ground true annotation into clusters on stochastic block models (SBM) with the size and density of the connectome better than the spectral methods related to simple random walks. Based on the cluster detectability threshold, we determined that the optimal number of modules in the connectome of *C.elegans* is seven, which, surprisingly, further provides the best agreement with the anatomical partition (the so-called ganglia). The discovered communities have a clear interpretation in terms of their functional role, which allows us to discern three groups of structural clusters in the worm: the brain group, movement controller, and information flow connector. Thus, our work provides a robust network-based framework to reveal mesoscopic structures in sparse connectome data, paving way to further investigations of connectome mechanisms for different functions.

## Introduction

Complexity of biological and social systems driven by collective behaviour of their agents is commonly studied using network (or graph) representation, where nodes represent agents and edges correspond to pairwise coupling between them. The resulting dimensionality reduction frequently allows to extract the most valuable information about hidden relationships governing static and dynamic properties of a system. One of the most striking and practically important examples of such information is the mesoscopic organization of agents into modules or communities.

The nervous system is no exception in this regard as it can be represented as a structural connectome, that is, a graph, where vertices are nerve cells and edges reflect direct structural connections (wiring) between them. Similarly to most real-world networks, the connectome is extremely sparse, that is, its number of theoretically possible connections between neurons greatly exceeds the factual amount of connections [1].

Such a reduction of excessive edges is a consequence of network *modularity*, a tendency to form assortative communities (modules) with relatively loose inter-connections. Like an effective team work of people where complex problem requires distribution of tasks among specialized groups of participants, mesoscopic organization of neurons in a connectome serves to facilitate certain functions of the nervous system, such as "wire together fire together" principle, [2]. Thus, accurate detecting of modules (communities) in the connectome data can help to establish a conversion between micro-level single neuron interactions and macro-level organism behaviour.

Community detection is an extremely hot topic in various fields such as technological [3, 4], biological [5, 6], social [7, 8] and economical [9–11] fields. A widely used approach in community detection is a spectral decomposition of a linear operator defined on a network: information about communities is then encoded in several leading eigenvectors [12, 13]. It was shown that all commonly used matrices (adjacency, Laplacian, modularity, non-backtracking, see Methods) readily classify nodes as long as network density is sufficient [14, 15]. In particular, the modularity operator is one of the most efficient instruments that successfully detects communities in stochastic networks of various nature [8, 16–18]. The modularity operator can be used to extract mesoscopic organization in *C.elegans* [19].

Sparse graphs are a special case where most of the traditional community detection methods suffer from fundamental limitations. Namely, at a given cluster strength there is a critical network density below which community detection becomes a very difficult problem [20]. Furthermore, traditionally used operators (adjacency, Laplacian, modularity) turn out to fail above this threshold, since their leading eigenvectors rapidly become uncorrelated with the intrinsic community structure upon decrease of network density. This behaviour is explained as the emergence of vertices with anomalously high degree (hubs), which eventually perturbs the spectral edge of these operators because of the "Lifshitz tails" of spectral density in sparse graphs ([21–23]). Localization on hubs, but not on true communities, is a major

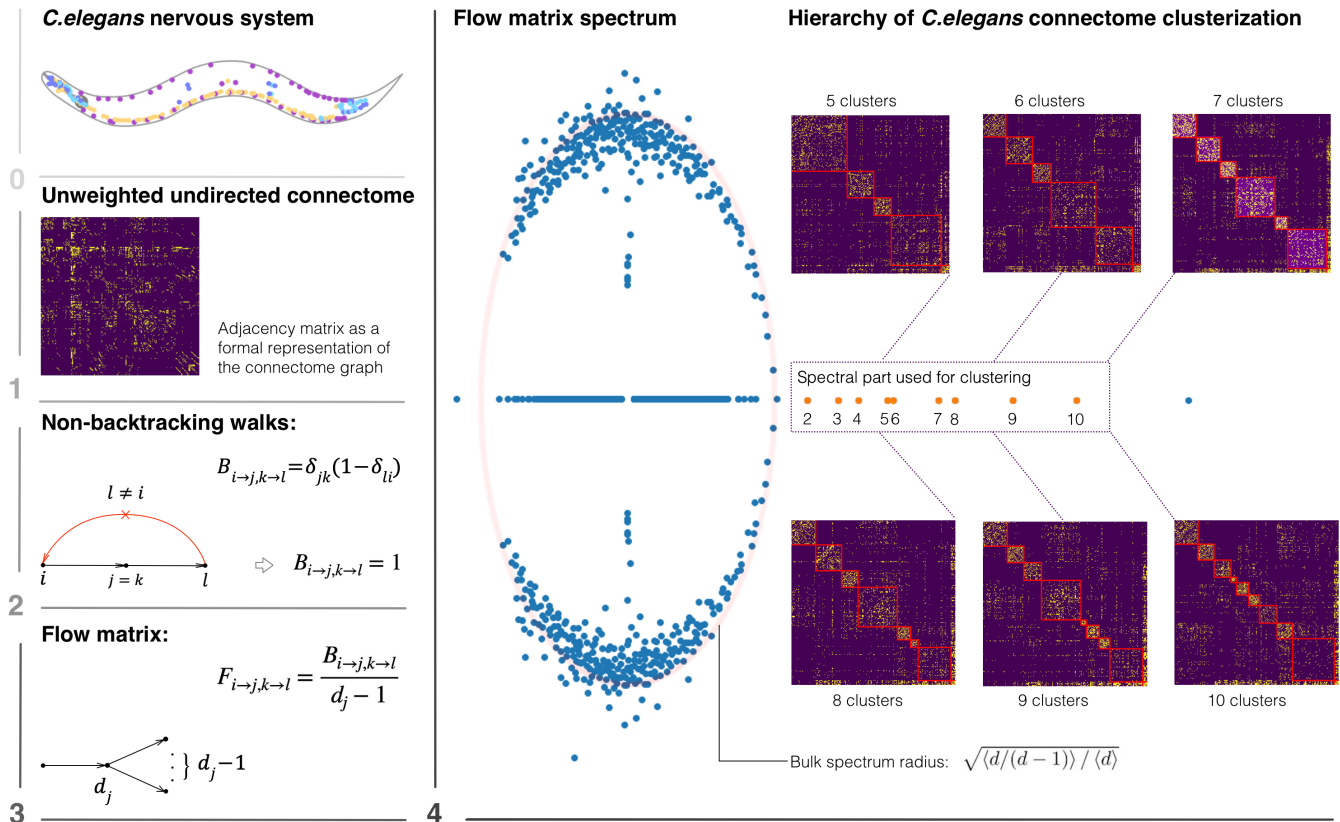


FIG. 1: Clusterization of *C.elegans* connectome by means of the spectrum of the non-backtracking flow matrix: **0**. A simplified scheme of the *C.elegans* nervous system; **1**. Representation of the connectome as the adjacency matrix; **2**. Constructing non-backtracking walks on the connectome network; **3**. Normalization by the out-degree towards the non-backtracking flow operator; **4**. Spectrum of the flow matrix with the orange dots representing eigenvalues outside of the spectral radius (pale red), which are used for identification of the communities.

drawback for all conventional spectral methods in the sparse regime.

To address this issue, Krzakala et al. proposed [20] to make use of the non-backtracking (Hashimoto) random walks on the associated directed graph. By construction, such walks cannot revisit the same node immediately at the following step and, as a result, they do not localize on hubs. The leading eigenvectors of the non-backtracking operator (the transfer matrix of non-backtracking walks) encode for the true community structure up to the theoretical resolution limit [20]. Due to their intrinsic ability to deal with sparse graphs, the non-backtracking walks have received increasing attention in the analysis of biological datasets. Recently we have shown that this approach allows to reveal compartments in chromosomes folding at the single-cell level from the single-nucleus Hi-C experiment [24].

In this work, we examined neuronal connectivity in *Caenorhabditis elegans* — the simplest organism with structural connectome first mapped by White et al. in 1986 [25], which has been completely described by now. Although relatively simple, the nervous system is a prominent part of *C. elegans* with almost one third of all the cells in its body being neurons. Importantly, the morphology, location and connectivity of each neuron are remarkably invariant across individuals [26], which makes this organism very convenient for studying neuronal connectivity and related functions. Curiously, due to the elongated shape of the nervous system stretched along the body of the worm, the adjacency matrix of the *C.elegans* connectome is similar to a single-cell chromosome contact map, which describes the spatial proximity of loci in individual chromatin trajectories [24, 27]. The so-called scaling in both types of data, being a generic polymer (or worm-like) effect, is a major source of sparsity of the corresponding matrices. This prompts one to apply to the *C.elegans* connectome the clustering procedures specifically designed for reliable detection of communities in sparse datasets.

Accordingly, we studied the mesoscopic organization of *C.elegans* connectome by means of the non-backtracking walks. Namely, we constructed the Newman’s flow operator, which describes the transfer probability of a random walk

on the associated directed connectome with prohibited immediate revisiting. The isolated part of the flow matrix spectrum is known to encode for communities and can be used by the clustering algorithm. We ran simulations of community detection on stochastic block models (SBMs) of the corresponding size and density as the connectome and demonstrated that the non-backtracking flow matrix outperformed all traditional operators, in the full agreement with asymptotic results of [20]. In particular, we show superiority of non-backtracking walks over the modularity operator, which was previously used for spectral clustering of the *C.elegans* connectome [19].

To reliably determine the amount of clusters in the network we realized an algorithm based on the theoretical detectability threshold for SBMs. Our network-based approach revealed seven detectable communities in the *C.elegans* connectome, which further yielded the maximal overlap with anatomically pre-defined groups of neurons (so-called ganglia). We interpreted each found cluster and showed that all clusters overlapped with certain ganglia or could be associated with specific functions. We made a statistical comparison of the clusters obtained by the non-backtracking method with partitions done by other approaches from the literature and found that the non-backtracking clusters were much better interpretable in terms of functions because they overlapped with the ganglia. Finally, we assessed functional and anatomical connectivity between the clusters and revealed three classes in the *C.elegans*: A. Worm Brain (ring neurons and head ganglia), B. Worm Movements Controller (ventral cord neural group), C. Worm Information Flow Connector (lateral ganglia).

### Stochastic block model and non-backtracking random walks

Here we provide a network theory background underlying clustering methods, which is instructive for the definition of the model, and connection with several widely used spectral clustering approaches is explained in the Methods section. Stochastic block model (SBM) is a commonly used benchmark for community detection in real-world networks, with several important theoretical results obtained for spectral clustering in this model [15, 16, 20, 28–30]. SBM is a generalization of an Erdős-Renyi random graph on  $N$  nodes, where the probability of an edge depends on particular pair of chosen vertices. First the nodes are split into  $k$  different groups (clusters),  $G_i, i = 1, 2, \dots, k$  and the edges between the pairs of vertices are then generated independently with a probability dependent on the cluster  $G_i$ . Generally, there is a matrix of pairwise cluster probabilities  $W = w_{rt}$  with  $(r, t) = 1, 2, \dots, k$ , such that a pair of nodes  $(i, j) : i \in G_r, j \in G_t$  is connected by an edge with probability  $w_{rt}$ . Thus, the corresponding entry in the adjacency matrix  $A_{ij}$  is 1 with probability  $w_{rt}$  and 0 otherwise. In the simplest version (so-called planted SBM), all off-diagonal elements of matrix  $W$  are equal to  $w_{out}$  and all diagonal elements are equal to  $w_{in}$

$$W_{rt} = \begin{cases} w_{in}, & r = t \\ w_{out}, & r \neq t \end{cases} \quad (1)$$

which corresponds to identical communities in the network. To obtain community structure (assortative communities) one should require  $w_{in} > w_{out}$ . In the connectome context, the neurons belonging to the same cluster have a preferentially higher probability to be connected with a link. Still, many of the nodes within the same cluster in the connectome are not directly connected (clusters are not cliques), allowing one to make use of stochastic models of cluster formation in the connectome.

Importantly, for SBMs there is a certain threshold on the minimally allowed difference  $\Delta w$  between  $w_{in}$  and  $w_{out}$  in order for the cluster structure to be resolved [15, 28]. Following conventional notation, let us introduce the rescaled cluster affinities,  $c_{in} = Nw_{in}$  and  $c_{out} = Nw_{out}$ , which scale linearly with the number of the inner and outer edges of a typical community. The detectability rule states that the clusters are asymptotically well resolved as long as

$$c_{in} - c_{out} > k\sqrt{c} \quad (2)$$

where  $c = \frac{c_{in} + c_{out}}{2}$  is the average of  $c_{in}, c_{out}$ . For dense networks  $c_{in}, c_{out}, c \sim O(N)$  and, thus, condition (2) is satisfied at any small  $\Delta w > 0$ . In the sparse case,  $c \sim O(1)$ , the threshold (2) provides the actual detectability limit on  $\Delta w$  and  $k$  of the cluster structure and should be carefully taken into account in practice.

Spectral methods, such as Laplacian, adjacency or modularity, have been widely used to recover community structure in relatively dense stochastic block model networks [12, 14, 16, 29–31]. The leading non-trivial eigenvectors of the corresponding operators provide dimensionality reduction of the system and these latent coordinates are then used by some conventional clustering algorithm (such as k-means) to perform partitioning into specified number of clusters [12]. However, as it was noted in [20], for sparse networks the leading eigenvectors become uncorrelated with true community structure above the theoretical threshold (2). This is because of the abundance of star-like sub-graphs (hubs) in a sparse network, which are identified by these operators instead of cyclic subgraphs associated with the internal structure of communities. Indeed, as these operators are related to random walks on a graph, true clusters interfere

with hubs in their spectrum. As a result, it turns out that the spectral methods that exploit random-walk-related operators (such as modularity, adjacency or Laplacian) fail to find communities in rather sparse networks, despite of the satisfied detectability condition (2).

To overcome this difficulty, the spectrum of the Hashimoto matrix  $B$  can be utilized, which is a transfer matrix of non-backtracking walks on a graph. It is defined on the edges of the directed graph,  $i \rightarrow j, k \rightarrow l$ , as follows

$$B_{i \rightarrow j, k \rightarrow l} = \begin{cases} 1 & \text{if } j = k \text{ and } l \neq i \\ 0 & \text{otherwise} \end{cases} \quad (3)$$

It is seen from (3) that the non-backtracking operator prohibits returns to the point which a walker visited at the previous step, thus effectively circumventing localization on the hubs. Notably, matrix  $B$  is non-symmetric and has a complex spectrum. For Poissonian graphs, the spectrum of  $B$  is constrained within a circle in the complex plane, whereas real eigenvalues of  $B$  lying out of the circle are relevant to the community structure even in sparse networks. Associating the corresponding eigenvectors with the network partitioning allows detecting communities all the way down to the theoretical limit (2). Interestingly, a "reluctant" version of the non-backtracking operator allows to explore the hanging trees of the network [31], which the original operator  $B$  ignores by construction.

In [29] the corresponding flow operator was proposed, which conserves the probability flow at each step of the non-backtracking walker (see Fig. 1)

$$F_{i \rightarrow j, k \rightarrow l} = \frac{\delta_{jk}(1 - \delta_{li})}{d_j - 1} \quad (4)$$

where  $d_j$  is the degree of the vertex  $j$ . While the powers of non-backtracking matrix  $B$  count the non-backtracking walks of particular length on a graph, the flow matrix  $F$  is the transfer matrix of the non-backtracking probability. Similarly to the non-backtracking matrix, the bulk of the eigenvalues of  $F$  lie onto the complex plane within a circle of radius

$$\sqrt{\frac{\langle d(d-1)^{-1} \rangle}{\langle d \rangle}} \quad (5)$$

but, as shown in [29], has a more clear edge of the spectral band. In what follows, we will use the flow matrix (4) for the purpose of the connectome clustering.

### Clustering the connectome of a worm: how many clusters are there?

The nervous system is by far the most complex part of the nematode *C.elegans* as the neurons constitute one third of all cells in this organism. After the pre-processing stage (see Methods), the connectome consists of  $N = 279$  vertices representing neurons and  $C = 2287$  edges between them representing structural connections. Since only 6% of the theoretically possible amount of edges are present in the network with fewer than 10 connections per a single cell, one may conclude that we deal with a rather sparse network.

In order to obtain communities in *C.elegans* connectome we implemented the spectral clustering approach, based on the leading non-trivial eigenvectors of the non-backtracking flow matrix (4). The spectrum of the actual network is shown in the Fig. 1. Interestingly, the isolated part of the flow spectrum consists of the maximal (trivial) eigenvalue and 9 smaller eigenvalues that lie on the real line outside the bulk, constrained by a circle of the radius (5). The corresponding eigenvectors correlate with the community structure and are used in the clustering approach.

We asked – and this is not trivial – what the optimal number of clusters would be that one could resolve in the data using the eigenvectors. We used an approach based on the detectability threshold (2). Here, a given mean cluster strength  $\Delta w$  the condition (2) establishes the maximum amount of clusters that can be theoretically resolved in the sparse network of given size  $N$  and the average link probability  $w$ . The critical number of clusters is related with the parameters of the network as follows

$$k_{max} = \frac{\Delta w}{w} \sqrt{N} \quad (6)$$

To find  $k_{max}$  in the *C.elegans* connectome we clustered the network into consecutive number of clusters  $k = 2, 3, 4, \dots, 10$  and compute  $c_{in}$  and  $c_{out}$  as averages over the detected clusters for each partition (see the sketch in Fig. 2b, explaining the procedure). A hierarchy of resulting community structures for different  $k$  is shown in Fig. 2c. As Fig. 2a clearly demonstrates up to  $k = 7$ , the detectability condition (2) is well satisfied. Thus, based on Fig. 2a, our algorithm

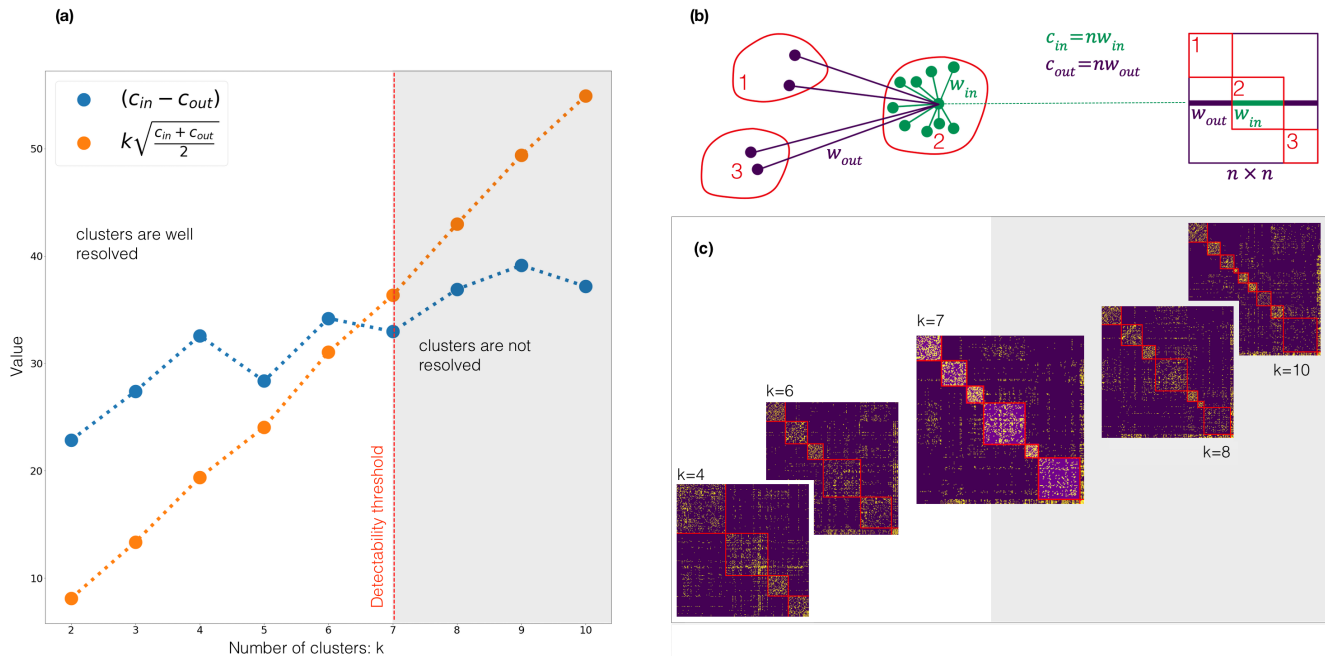


FIG. 2: (a) Graphical representation of the condition (2) as a criterion for the optimal number of clusters resolving. (b) A sketch of the  $c_{in}$  and  $c_{out}$  computation procedure. (c) Hierarchy of resulting *C.elegans* connectome community structures for different  $k$  obtained by the flow matrix operator.

suggests that the optimal amount of clusters in the connectome lies between  $k = 6$  and  $k = 7$ , so we further used value of  $k = 7$  for the subsequent analysis.

Surprisingly, we found that the overlap between the obtained partitions for different  $k$  and the anatomic partitions into ganglia has the maximum at  $k = 7$ , Fig. 3c (green curve). We measured the agreement between various partitions by means of the adjusted mutual information (AMI, see Methods). Despite the ganglia were not expected to provide the absolute ground truth for the clusters of the structural connectome, the very fact that  $k = 7$  clusters provided the best agreement with the anatomic partition supports the proposed network-based inference approach and provides cross-validation to the optimal number of clusters that could be resolved in the *C.elegans* connectome.

Having found the detectability threshold which was explicitly limiting the number of detectable clusters, applying other clustering operators was the next logical step in the analysis, including the traditional community detection methods such as Laplacian, normalized Laplacian, and modularity matrix together with suggested  $k = 7$ . The clusters obtained from different operators were compared with the biological benchmarks in the same way as we did it for the flow matrix (Fig. 3).

### Non-backtracking flow and normalized Laplacian operators outperform modularity on simulated connectomes

Having found the optimal amount of clusters, we reiterated to the question of the operator that would be most appropriate for clustering this kind of network. For that we generate a family of stochastic block models with blocks similar to what we have obtained in the *C.elegans* connectome. Namely, we fixed the network size,  $N = 279$ , the outer-cluster probability,  $w_{out} = 0.034$ , and the total number of clusters,  $k = 7$ . Furthermore, the sizes of the simulated blocks were chosen to recapitulate the sizes of the inferred clusters in the original data. The only parameter subject to variation was the inner-cluster probability,  $w_{in} = \{0.05, \dots, 0.157, \dots, 0.6\}$ . For each value of  $w_{in}$  we generated 200 random matrices and ran the spectral clustering on the leading eigenvectors of four operators: non-backtracking flow, normalized Laplacian, Laplacian and modularity.

The partitions predicted by the four operators were then assessed using AMI scores, see Fig. 3a. The results clearly demonstrated the superiority of non-backtracking flow and normalized Laplacian for clustering of the simulated SBMs. The flow operator slightly outperformed the normalized Laplacian, especially in the region of intermediate relative cluster strengths,  $w_{in}/w_{out}$ . Such a moderate effect was the result of a small network size, while in the limit of large networks the non-backtracking operator is known to be superior [20]. Notably, the empirical value of

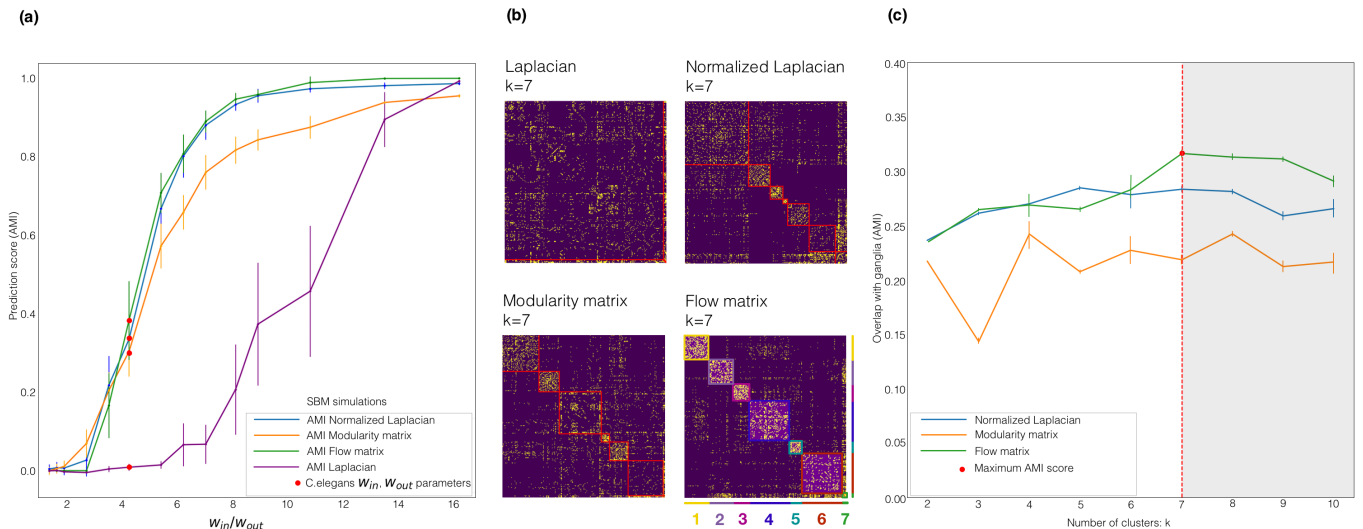


FIG. 3: (a) Mean AMI score assessing of the SBMs partitions predicted by the four different operators. Red dots correspond to the SBMs simulated with the empirical  $w_{in}/w_{out}$  parameters obtained from the connectome. (b) Partitions of the *C.elegans* connectome into  $k = 7$  clusters obtained by different spectral methods. Each of the seven clusters detected by flow operator were assigned With a unique color. (c) Assessed similarity between ganglia and predicted partitions using the AMI score. The red dot denotes the maximal AMI score value. The graph corresponding to Laplacian clusters overlap with ganglia was excluded from the picture, because resulting AMI was equal to 0 everywhere.

$w_{in}/w_{out} = 0.157/0.037 \approx 4.2$ , labeled on a graph Fig. 3a by red dots on the AMI curves, corresponds to the edge of cluster detectability as in this region AMI is abruptly decaying to zero. For large  $N$  there is an associated phase transition [15, 28], thus, one can call the empirical connectome critical. In fact, this is the result of the critical amount of clusters, chosen in accordance with the detectability condition (2) above. Intermediate values of the prediction score manifest the balance between accurate restoration of the clustering structure and resolving the maximal possible amount of clusters.

Importantly, the superiority of non-backtracking flow is independently evident in the comparison of AMI scores between ganglia and clusters resolved by the different operators, Fig. 3c. At  $k = 7$ , AMI score for the non-backtracking flow was the highest among all the methods, yielding similar values as produced by the normalized Laplacian, which agrees well with the prediction score analysis on stochastic block models, Fig. 3a.

Put together, this simulation and network analyses suggest that the non-backtracking flow operator is superior over the conventional spectral clustering approaches on networks of size and composition similar to the *C.elegans* connectome.

### Biological interpretation of clusters

*Seven ganglia out of ten significantly overlap with the structural modules*

It would be reasonable to suggest that the presence of enhanced clustering would be functionally important to improve information flow in a biological network that evolved under intense competition for survival. For tackle a biological interpretation, we first used the partitioning of the worm nervous system into ganglia as a benchmark. As discussed above, the overlap between the clusters obtained by the flow matrix and the ganglia is maximal at seven clusters (Fig. 3). We next examine how the seven clusters were related to the ganglia in more detail and calculate the pairwise intersections between the ten ganglia and each of the seven clusters (Fig. 5a). Conspicuously, seven ganglia out of ten had a statistically significant overlap with at least one flow matrix cluster ( $p \leq 10^{-5}$ ). For the other three ganglia (1 – posterolateral, 6 – dorsal and 7 – retrovesicular), the statistical significance was noticeably lower ( $p \leq 10^{-2}$ ). The fact that the number of matched ganglia was equal to the optimal number of clusters could indicate a one-to-one correspondence between the anatomical and structural partitions. Yet, as one can infer from 5a, there were two ganglia (4 – lateral and 8 – ventral cord) that intersected with two clusters (3rd, 7th and 8th, 6th,

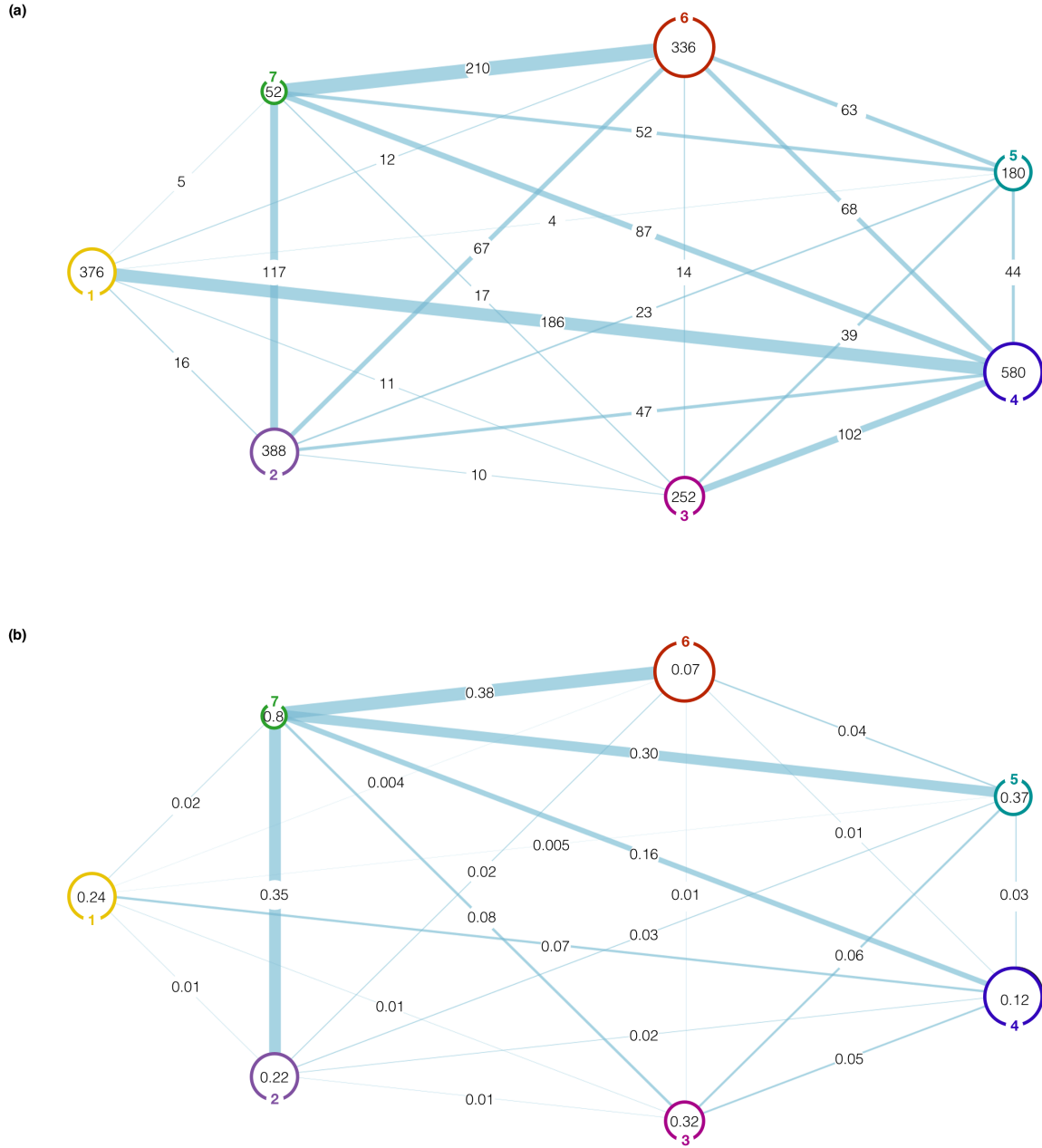


FIG. 4: (a) Mesoscopic representation of the *C.elegans* network, in terms of connectivity of the clusters. The size of each circle is proportional to the number of neurons in the corresponding cluster. The number inside each circle equals to the in-cluster amount of edges and the thickness of each line is proportional to the amount of edges between the respective clusters. (b) A complimentary representation of the network in terms of in-cluster/out-cluster connection probabilities. All numbers are normalized to the total number of edges within or between the clusters.

respectively) with p-value  $p \leq 10^{-5}$ . Furthermore, all flow matrix clusters, except two (the 5th and 7th), had some ganglia in significant intersection; the 6th cluster intersected significantly with four ganglia.

We further turned to different partitions of *C.elegans* previously reported in the literature. Namely, we take two open-source annotations obtained by two other algorithms: iterative modularity maximization (IMMA) [32] and Erdos-Renyi mixture model (ERMM) from [33]. The IMMA approach is based on maximization of modularity score (6 groups were found for the weighted connectome), while the ERMM is a non-deterministic algorithm that fits arbitrary,

not planted, SBM to the network (9 groups were found). As Table 1 indicates, the global AMI score between the ganglia and flow matrix clusters was 0.34 and coincided with the score for the ERMM algorithm. At the same time, the IMMA algorithm yielded a slightly worse agreement with the ganglia with an AMI score of 0.31. Importantly, all three algorithms produced structural partitions that were more similar to each other in the AMI metric than to the ganglia, which provided anatomic partitioning. Thus, despite structural partitions were notably different from the anatomic one, the flow matrix and ERMM were more consistent with the ganglia partitioning than IMMA globally.

A more detailed analysis between particular ganglia and clusters revealed that the 1st, 6th, and 7th ganglia in the ERMM and IMMA partitions did not have a structural cluster with a significant overlap ( $p \leq 10^{-5}$ ), being in full agreement with the conclusion drawn on the base of flow matrix clusters. Such robust consistency between the three different approaches indicates that posterolateral, dorsal and retrovesicular ganglia are weakly related to structural connectome modules. In this context, the flow matrix brought a clear added value, since it revealed two additional ganglia – the 2nd (ventral) and the 5th (dorsorectal) – that were associated with particular structural clusters, which were absent in the other two methods.

*Neurons of different functional types correspond to particular structural modules*

As a second biological benchmark, we consider the partitioning of the *C.elegans* nervous system into five groups corresponding to different neuronal functions: sensory neurons (S), polymodal neurons (P), interneurons (I), command neurons (C) and motoneurons (M). Noticeably, each functional type was found to be located within a particular structural cluster ( $p \leq 10^{-5}$ ), as derived by the flow matrix 5b. This was in sharp contrast with the results of the other two approaches. The ERMM method did not cluster the polymodal neurons, whereas the IMMA method did not cluster polymodal and command neurons.

The above analysis demonstrates that all flow matrix clusters, except of the 5th and the 7th, can be associated with their particular ganglia. Here we find that the 5th cluster corresponds to the interneurons (I) and apparently captures their particular function, which is not obviously mapped onto anatomical position. The 7th cluster consists of almost all command neurons of the worm (six from the lateral ganglion and two from the lumbar ganglion). We also note that the 6th flow matrix cluster, which overlaps with four different ganglia simultaneously, has a moderate but relatively significant number of motoneurons (M). As we shall see below, the 2nd and 6th clusters actually respond to the worm movements.

*Cross-talk between the clusters is determined by neuronal programs*

On the basis of the complementary nature of detected communities (functional roles and anatomical locations), we identify the groups of clusters. The absolute values of the pairwise edges between the clusters (see Fig. 4a) and the corresponding probabilities of making an edge between each two neurons (see Fig. 4b) characterize the extent of cross-talk between the clusters. Below, we suggest a classification into three groups of clusters, which are stabilized by similar functions and/or 3D positions: 1st and 4th; 2nd and 6th; 3rd, 5th and 7th. It should be noted that the neurons listed below are the names of neuron sets, for example, VA contain twelve individual neurons VA1-VA12 or ADA contain ADAL and ADAR, for detailed enumeration of cluster elements, see Fig. 6.

- Worm Brain (1st and 4th clusters)

Similarly to the multifunctional organization of the brain of more complex organisms, we found that neurons in these two clusters had a common anatomical position and were involved in complex multimodal processes [25]. According to the corresponding 3D model (see Fig 6), it can be judged that the 1st cluster is closer to the nose of the worm and the 4th cluster is located behind it. This anatomical attitude between clusters is consistent with the functions, the distribution of which is uneven across the neurons of these clusters. Accordingly, all polymodal neurons of the head part of the worm (IL1, IL1D, IL1V, OLQD, OLQV, RIM, ASH) and anterior ganglion sensory neurons (IL2D, IL2, IL2V, OLL) are located in the 1st cluster, while the majority of interneurons (ADA, RIA, RIB, RIF, RIG, RIH, RIR, RIS, RIV, URB, URX, SAAD, SAAV, AVK, SDQ, SIAD, SIAV, SIBD, SIBV) belong to the 4th cluster. Such a "layered" organization is consistent with intuition about how the accepted by the worm's nervous system external signals should be processed. From the perspective of the compressed connectome view (Fig. 4), clearly seen, that most of the contacts from the 1st cluster ( $\approx 80\%$ ) connect it with the 4th cluster which in turn has high contact probability ( $\approx 16\%$ ) with the smallest and full of command neurons 7th cluster. This fact could mean that the pair of 1st and 4th clusters plays the roles of acceptor and preprocessor of the sensory information flow with subsequent signal transmission to command neurons in 7th

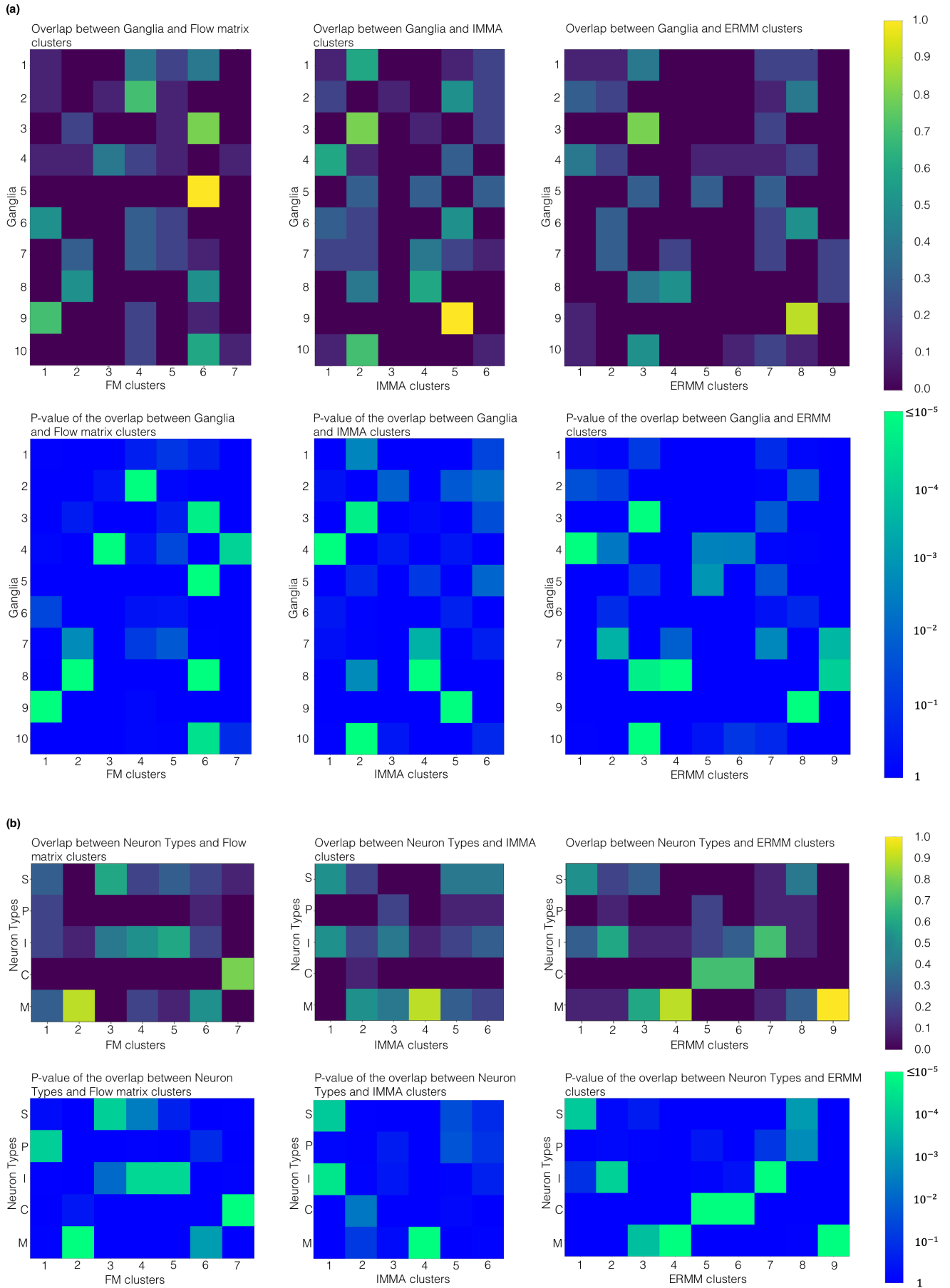


FIG. 5: **(a)** Overlaps and p-values between the clusters and ganglia. **(b)** Overlaps and p-values between the clusters and neuronal types: sensory neurons (S), polymodal neurons (P), interneurons (I), command neurons (C), motoneurons (M). For both **(a)** and **(b)** each column represents specific clusterization method: flow matrix, iterative modularity maximization algorithm (IMMA) [32], Erdos-Renyi Mixture Model (ERMM) [33].

|  | AMI score |
|--|-----------|
| Ganglia vs Flow Matrix clusters            | 0.34      |
| Ganglia vs IMMA clusters [32]              | 0.31      |
| Ganglia vs ERMM clusters [33]              | 0.34      |
| Flow Matrix clusters vs IMMA clusters [32] | 0.4       |
| Flow Matrix clusters vs ERMM clusters [33] | 0.45      |
| IMMA clusters [32] vs ERMM clusters [33]   | 0.41      |

TABLE I: Overlap between various modular structures

cluster in order to further correction of motor programs, through the dense contacts of the 7th cluster with in 2nd and 6th clusters.

- Worm Movements Controller (2nd and 6th clusters)

These two clusters contain the ventral cord neural group, which is split between them according to the anatomical positions of the neurons: neurons in the head half fall into the 2nd cluster, while neurons in the tail body half fall into the 6th cluster (Fig. 6).

Together, almost 70% of these two clusters neurons belong to the ventral cord (AS, DA, DB, DD, VA, VB, VC, VD, AVE), which motoneurons are located along the entire body of the worm and split exactly into two groups in accordance with which half of the body of the worm these neurons belong to.

The remaining 23% are represented by neurons of the tail ganglia: lumbar ganglion, pre-anal ganglion, and dorsorectal ganglion (PHA, PHB, PHC, PLM, PLN, PVD, PVN, PVQ, PV, LUA, PWV, PDA, PDB, DVA, DVB, DBC) and belong to the 6th cluster, which is responsible for the tail part of the ventral cord and 7% are outliers see (Fig. 5a). Excitatory motor neurons in the ventral cord function as motor rhythm generators and underlie body undulation during reversal and forward movements [34]. That is why we chose to name this pair as a *worm movements controller*. The connection probability between these two clusters is significantly low ( $\approx 2\%$ ), which is tenable if we interpret them as two parts of the movement control system and the dense connections between the motoneurons from opposite parts of the worm body are not functionally significant. At the same time, the high probability of connection between these two clusters and the 7th one ( $\approx 35\%$ ,  $\approx 38\%$ ), which consist of command neurons, is agree with the notion that command neurons are responsible for coordinating the movements of the worm (Fig. 4).

- Worm Information Flow Connector (3rd, 5th and 7th clusters)

Almost 75% of the neurons in these three clusters belong to the lateral ganglion: sensory neurons (ADF, ADL, ASE, ASG, ASH, ASI, AFD, AWA, AWB, AWC, ASJ, ASK), interneurons (AIA, AIB, AIN, AIY, AIZ, AUA, AVH, AVJ) and command neurons (AVA, AVB, AVD, PVC). Command neurons, which are all located in the 7th cluster, by definition receive a convergence of integrative sensory inputs and output to a multifarious group of pattern-generating efferent neurons [35]. This is consistent with the contact probabilities between the 7th cluster and the Worm Movements Controller (Fig. 4b). For example, there are evidences that the ablation of AVB or AVA command neurons led to the impairment of spontaneous forward or backward movements, establishing them as the most critical regulators for directional motion [36]. Therefore, it can be assumed that the 7th cluster is some kind of command center coordinating the work of clusters 2nd and 6th, and responsible for the implementation of the worm's motor programs.

In terms of sensory neurons and interneurons of the lateral ganglion, located in the 3rd and 5th clusters, it should be noted that the vital role of the lateral ganglion consists of the processing of information and providing an essential connection between the sensory and motor components of the *C.elegans* nervous system [37]. The distribution of contacts between the 7th command cluster and other clusters clearly shows its significant role in the information flow integration processes: from the interneurons located in the 3rd, 4th and 5th clusters (Fig. 5b), it receives information about the outer environment and coordinates the behavior of the worm through dense contacts with the worm movements controller.

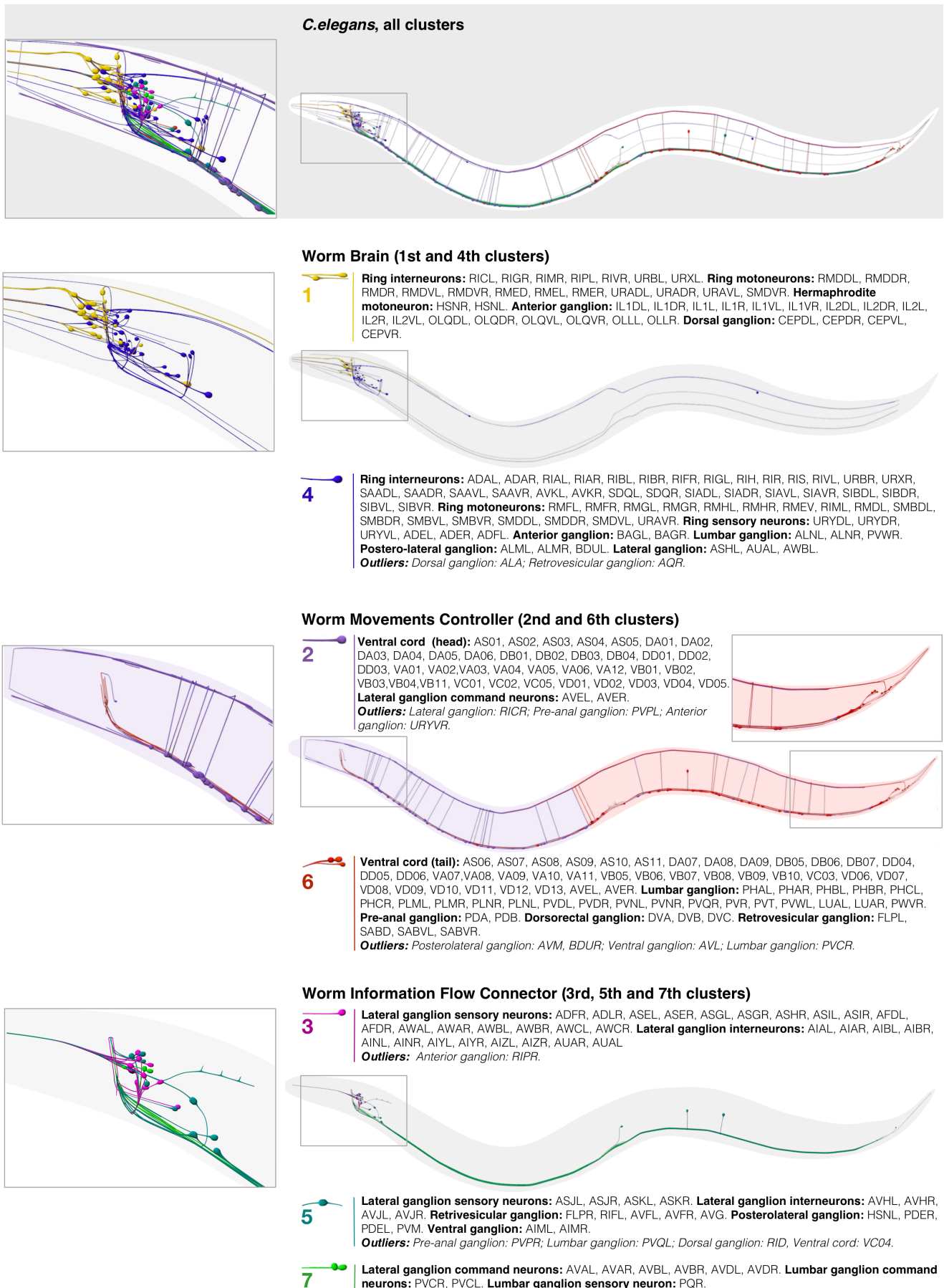


FIG. 6: Three-dimensional visualization of the detected clusters in the connectome. On the basis of the complementary analysis of functional roles and anatomical locations, we identify three groups of clusters. Original 3D coordinates were taken from the Caltech Wormbase project [38].

## I. CONCLUSIONS

In this paper, we performed a detailed analysis and demonstrated applicability of the spectrum of non-backtracking random walks to the problem of the structural connectome clustering on the model example of *C.elegans*. This clusterization method had a deterministic nature and simple computational implementation. Based on the theoretical detectability threshold we determined that the optimal number of clusters in the connectome was seven, which has further yielded the best agreement with the anatomical partitions of the neurons (the so-called ganglia). The non-backtracking flow operator produced the partitions that better correlated with biological benchmarks in the worm than other traditional methods (deterministic or iterative nondeterministic algorithms) used in the literature so far.

The non-backtracking flow operator decomposed the *C.elegans* connectome network into seven interpretable communities: two multifunctional head clusters full of ring neurons, two modules responsible for movements control in the head and tail halves of the worm, one cluster full of the command neurons and two clusters belonging to the lateral ganglion consisting of sensory neurons and interneurons. Biological interpretation of the found clusters suggests that all ganglia, except of two (posterolateral and dorsal), have statistically significant overlap with the structural modules. Importantly, this finding is consistent with structural partitions performed by previously used approaches, suggesting that these two anatomic regions *mediate* propagation of information from other modules. Furthermore, in contrast to previously used approaches, the non-backtracking operator revealed two new ganglia (ventral and dorsorectal) that exhibited a significantly stronger overlap with the structural modules. Our integrative analysis of functional and anatomical connectivity of the optimal clusters allowed us to dissect three neuronal classes: the worm brain, the worm movements controller, and the worm information flow controller.

In summary, our study uncovers the existence of hidden relationships between mesoscopic structure, functions and anatomical locations of the neurons that define and control the behaviour of an organism. However, to derive these relationships one needs to reliably resolve the modules in the structural connectome data. In the framework of the simplest model organism our work explicitly demonstrates that the mesoscopic structure of the connectome should be investigated by taking into account intrinsic sparsity of the network. Given universality of our approach, we suggest that it can be further extended for connectome studies of more complex organisms.

- 
- [1] Brian Karrer, Mark EJ Newman, and Lenka Zdeborová. Percolation on sparse networks. *Physical review letters*, 113(20):208702, 2014.
  - [2] Donald O Hebb. The first stage of perception: growth of the assembly. *The Organization of Behavior*, 4:60–78, 1949.
  - [3] R. Albert, H. Jeong, and A.L. Barabási. Internet: Diameter of the world-wide web. *Nature*, 401(6749):130, 1999.
  - [4] A. Broder et al. Graph structure in the web. *Computer networks*, 33(1-6):309–320, 2000.
  - [5] J. Dekker, M. A. Marti-Renom, and L. A. Mirny. Exploring the three-dimensional organization of genomes: interpreting chromatin interaction data. *Nature Reviews Genetics*, 14(6):390, 2013.
  - [6] E. Ravasz, A. L. Somera, D. A. Mongru, Z. N. Oltvai, and A. L. Barabási. Hierarchical organization of modularity in metabolic networks. *Science*, 297(5586):1551–1555, 2002.
  - [7] S. Redner. How popular is your paper? an empirical study of the citation distribution. *The European Physical Journal B-Condensed Matter and Complex Systems*, 4(2):131–134, 1998.
  - [8] J. Chen, O. R. Zaiane, and R. Goebel. Detecting communities in social networks using max-min modularity. *Proceedings of the 2009 SIAM international conference on data mining*, pages 978–989, 2009.
  - [9] C. Piccardi, L. Calatroni, and F. Bertoni. Communities in italian corporate networks. *Physica A: Statistical Mechanics and its Applications*, 389(22):5247–5258, 2010.
  - [10] K. Polovnikov, V. Kazakov, and S. Syntulsky. Core-periphery organization of the cryptocurrency market inferred by the modularity operator. *Physica A: Statistical Mechanics and its Applications*, 540:123075, 2020.
  - [11] K. Polovnikov, N. Pospelov, and D. Skougarevskiy. Ownership concentration and wealth inequality in Russia. *Proceedings of the 31st International Joint Conference on Artificial Intelligence*, 2022.
  - [12] Ulrike Von Luxburg. A tutorial on spectral clustering. *Statistics and computing*, 17(4):395–416, 2007.
  - [13] M. Krivelevich and B. Sudakov. The largest eigenvalue of sparse random graphs. *Combinatorics, Probability and Computing*, 12(1):61–72, 2003.
  - [14] R. R. Nadakuditi and M. E. Newman. The largest eigenvalue of sparse random graphs. *Physical review letters*, 108(18):188701, 2012.
  - [15] A. Decelle, F. Krzakala, C. Moore, and L. Zdeborová. Inference and phase transitions in the detection of modules in sparse networks. *Physical Review Letters*, 107(6):065701, 2011.
  - [16] M. Newman. Finding community structure in networks using the eigenvectors of matrices. *Physical review E*, 74(3):036104, 2006.
  - [17] H. K. Norton et al. Detecting hierarchical genome folding with network modularity. *Nature Methods*, 15(2):119, 2018.
  - [18] M. Sales-Pardo, R. Guimera, A. A. Moreira, and L. A. N. Amaral. Extracting the hierarchical organization of complex systems. *Proceedings of the National Academy of Sciences*, 104(39):15224–15229, 2007.

- [19] R.K. Pan, N. Chatterjee, and S. Sinha. Mesoscopic organization reveals the constraints governing *Caenorhabditis elegans* nervous system. *PLoS One*, 5(2):e9240, 2010.
- [20] Florent Krzakala, Christopher Moore, Elchanan Mossel, Joe Neeman, Allan Sly, Lenka Zdeborová, and Pan Zhang. Spectral redemption in clustering sparse networks. *Proceedings of the National Academy of Sciences*, 110(52):20935–20940, 2013.
- [21] J. Reichardt and S. Bornholdt. Statistical mechanics of community detection. *Physical Review E*, 74(1):016110, 2006.
- [22] A. Arenas, A. Fernandez, and S. Gomez. Analysis of the structure of complex networks at different resolution levels. *New Journal of Physics*, 10(5):053039, 2008.
- [23] S. K. Nechaev and K. Polovnikov. Rare-event statistics and modular invariance. *Physics-Uspekhi*, 61(1):99, 2018.
- [24] K. Polovnikov, A. Gorsky, S. Nechaev, V. Razin, and S. V. Ulianov. Non-backtracking walks reveal compartments in sparse chromatin interaction networks. *Scientific Reports*, 10(1):1–11, 2020.
- [25] John G White, Eileen Southgate, J Nichol Thomson, Sydney Brenner, et al. The structure of the nervous system of the nematode *caenorhabditis elegans*. *Philos Trans R Soc Lond B Biol Sci*, 314(1165):1–340, 1986.
- [26] David H Hall and Richard L Russell. The posterior nervous system of the nematode *caenorhabditis elegans*: serial reconstruction of identified neurons and complete pattern of synaptic interactions. *Journal of Neuroscience*, 11(1):1–22, 1991.
- [27] T. Nagano et al. Single-cell hi-c reveals cell-to-cell variability in chromosome structure. *Nature*, 502(7469):59–64, 2013.
- [28] Aurelien Decelle, Florent Krzakala, Cristopher Moore, and Lenka Zdeborová. Asymptotic analysis of the stochastic block model for modular networks and its algorithmic applications. *Physical Review E*, 84(6):066106, 2011.
- [29] M. Newman. Spectral community detection in sparse networks. *arXiv preprint arXiv:1308.6494*, 2013.
- [30] Mark EJ Newman. Modularity and community structure in networks. *Proceedings of the national academy of sciences*, 103(23):8577–8582, 2006.
- [31] A. Singh and M. D. Humphries. Finding communities in sparse networks. *Scientific reports*, 5(1):1–7, 2015.
- [32] Raj Kumar Pan, Nivedita Chatterjee, and Sitabhra Sinha. Mesoscopic organization reveals the constraints governing *caenorhabditis elegans* nervous system. *PloS one*, 5(2):e9240, 2010.
- [33] Dragana M Pavlovic, Petra E Vértés, Edward T Bullmore, William R Schafer, and Thomas E Nichols. Stochastic blockmodeling of the modules and core of the *caenorhabditis elegans* connectome. *PloS one*, 9(7):e97584, 2014.
- [34] Quan Wen, Shangbang Gao, and Mei Zhen. *Caenorhabditis elegans* excitatory ventral cord motor neurons derive rhythm for body undulation. *Philosophical Transactions of the Royal Society B: Biological Sciences*, 373(1758):20170370, 2018.
- [35] Taizo Kawano, Michelle D Po, Shangbang Gao, George Leung, William S Ryu, and Mei Zhen. An imbalancing act: gap junctions reduce the backward motor circuit activity to bias *c. elegans* for forward locomotion. *Neuron*, 72(4):572–586, 2011.
- [36] Stephen R Wicks, Chris J Roehrig, and Catharine H Rankin. A dynamic network simulation of the nematode tap withdrawal circuit: predictions concerning synaptic function using behavioral criteria. *Journal of Neuroscience*, 16(12):4017–4031, 1996.
- [37] Nivedita Chatterjee and Sitabhra Sinha. Understanding the mind of a worm: hierarchical network structure underlying nervous system function in *c. elegans*. *Progress in brain research*, 168:145–153, 2007.
- [38] Todd W Harris, Igor Antoshechkin, Tamberlyn Bieri, Darin Blasiar, Juancarlos Chan, Wen J Chen, Norie De La Cruz, Paul Davis, Margaret Duesbury, Ruihua Fang, et al. Wormbase: a comprehensive resource for nematode research. *Nucleic acids research*, 38(suppl.1):D463–D467, 2010.
- [39] Beth L Chen, David H Hall, and Dmitri B Chklovskii. Wiring optimization can relate neuronal structure and function. *Proceedings of the National Academy of Sciences*, 103(12):4723–4728, 2006.
- [40] Lav R Varshney, Beth L Chen, Eric Paniagua, David H Hall, and Dmitri B Chklovskii. Structural properties of the *caenorhabditis elegans* neuronal network. *PLoS computational biology*, 7(2):e1001066, 2011.
- [41] ZF Altun and DH Hall. Handbook of *c. elegans* anatomy. *WormAtlas*. <http://www.wormatlas.org/handbook/contents.htm>, 2005.
- [42] Mark EJ Newman and Michelle Girvan. Finding and evaluating community structure in networks. *Physical review E*, 69(2):026113, 2004.

### Acknowledgements

All authors thank A. Gorsky, K. Anokhin, S. Nechaev, O. Valba and N. Pospelov for stimulating discussions on the project and A. Moiseeva for help with illustrations. The work of KP on the development of the spectral algorithm for the connectome analysis was supported by the Analytical center under the RF Government (subsidy agreement 000000D730321P5Q0002, Grant No. 70-2021-00145 02.11.2021). AO, AC and KP acknowledge the support of Idea Foundation grant in collection and analysis of the connectome data.

### Competing interests

The authors declare no competing interests.

## Code availability

Source code and data available on GitHub project page.

## Methods

### Data

We have worked with open-access data from the *C.elegans* connectome analysis project [39, 40]. It is an updated and revised version of the wiring data originally published in [25]. Neuron interactions, locations, sensory endings, and neuromuscular junctions, as well as the structure of the connectome, have been well studied and have been found to be invariant with respect to the type of animal [25, 26]. Connectome 3D model used for the reconstruction of cluster elements anatomical positions was taken from the Caltech Wormbase project [38].

The connectome is a network with 302 vertices and 2990 edges: 796 edges are formed by gap junctions only; 1962 contain only chemical synapses; 232 edges have both gap junctions and chemical synapses present. The entire nervous system is broken down into two large disconnected components and three isolated neurons (VC06, CANL, CANR). Twenty of the neurons in one of the components are located within the worm pharynx, which has its own separate nervous system, and the remaining 279 neurons (excluding three isolated neurons) are located in various ganglia along the worm body. During the preprocessing stage, all connections in the connectome are made undirected and unweighted. Furthermore, we did not divide the graph into two subgraphs according to contact types (chemical synapses or gap junctions) and analyzed the connectome in its entirety.

There is a large body of knowledge on individual neurons that produce node-wise features. In this work, we use the classification of neurons into ten anatomically defined ganglia (posterolateral, ventral, pre-anal, lateral, dorsorectal, dorsal, retrovesicular, ventral cord, anterior and lumbar ganglia) and five functional groups (sensory, polymodal, interneurons, command neurons, motoneurons) [41].

### From stochastic block model to non-backtracking random walks

One of the most popular methods for community detection (in particular, of the connectome [32]) is optimization of modularity. In fact, it can be shown that the generalized modularity functional provides the entropy of a Poisson weighted stochastic block model with quenched degrees (configuration model). Such models, for example, describe the results of single-cell contact counting experiments in chromatin networks, as was shown by us recently [24]. If the degrees of all vertices  $d_i = \sum_j A_{ij}$  are kept fixed, without additional imposed cluster structure, the expected weight of the edge under random degree-preserving randomization is simply  $P_{ij} = \frac{d_i d_j}{\sum_i d_i}$  for  $i \neq j$ . Assuming that the stochastic blocks are superimposed over the configuration model, each entry  $A_{ij}$  of the adjacency matrix of the observed network becomes a Poisson random variable with the mean  $P_{ij} w_{rt}$ , such that the nodes  $i$  and  $j$  are assigned to the groups  $G_r$  and  $G_t$ , respectively. Thus, the total statistical weight of  $A$  conditioned on the cluster probability matrix  $W$ , quenched degrees  $d_i$  and group labels  $g_i$  can be factorized into the product of the Poisson probabilities and written down as follows

$$\mathcal{Z}(A|W, d_i, g_i) = \prod_{i < j} \frac{P_{ij} w_{g_i g_j}^{A_{ij}}}{A_{ij}!} \exp(-P_{ij} w_{g_i g_j}) \quad (7)$$

which produces the following entropy

$$S_{conf.} \propto \log \mathcal{Z}(A|W, d_i, g_i) = \sum_{i < j} (A_{ij} - \gamma P_{ij}) \delta_{g_i g_j} \quad (8)$$

where  $\gamma$  is some parameter that depends on  $w_{in}$  and  $w_{out}$  of the planted SBM (1) as follows

$$\gamma = \frac{w_{in} - w_{out}}{\log w_{in} - \log w_{out}} \quad (9)$$

Clearly, the entropic functional (8) up to the parameter  $\gamma$  is nothing but the *modularity functional*, which is widely used in clustering tasks, for connectome clustering as well [32]. It is important to note that generally the parameter  $\gamma$

have to be chosen self-consistently with the cluster parameters of the partition (9), for which the iterative procedure has been recently proposed [24].

Modularity optimization has been originally proposed and proved to be useful for clusterization of scale-free networks, since, as we have shown above, it explicitly conserves the scale-free property of the degree distribution under stochastic randomization. Although most of the real-world networks are scale-free, modularity is one of the most popular approaches in spectral clustering. However, if one relaxes the degrees preservation assumption, the background probability becomes uniform  $P_{ij} = p$  and the underlying graph is assumed to be simply a  $G(N, p)$  Erdos-Renyi graph. Then the second term in (8) does not depend on cluster labels of the nodes, and maximization of the entropy for a given amount of clusters corresponds to maximization of the adjacency functional

$$S_{ER} \propto \log \mathcal{Z}(A|W, g_i) = \sum_{i < j} A_{ij} \delta_{g_i g_j} \quad (10)$$

which is trying to maximize the internal weight of the clusters. In a more general problem setting of a manifold learning, one is looking for the optimal representation (embedding) of  $N$  vertices in a low-dimensional space described by a set of coordinates  $g_i, i = 1, 2, \dots, N$  (suppose, the latent space is one-dimensional for simplicity). As long as close points in the original high-dimensional space should be eventually put close in the latent space, the natural functional to be minimized is

$$S_{ML} \propto \log \mathcal{Z}(A|W, g_i) = \frac{1}{2} \sum_{i \neq j} A_{ij} (g_i - g_j)^2 \quad (11)$$

which can be written as a quadratic form of the graph Laplacian,  $L = D - A$

$$S_{ML} \propto \sum_{i,j} L_{ij} g_i g_j \quad (12)$$

Of course, a similar functional over latent coordinates can be written for the modularity functional (8) as well.

Thus, we see that statistical inference of the optimal cluster structure is associated with optimization of a certain functional over partition of graph nodes. However, finding the global maximum of (8),(10),(12) is a very difficult computational task. To overcome this difficulty, spectral methods are used, which rely on the fact that the most essential information about the optimal partition is encoded in the first non-trivial eigenvectors of the corresponding operator. Indeed, the quadratic form associated with the manifold learning problem can be approximated by projecting the coordinates to the leading eigenvectors of the operator.

### Modularity matrix

In [42] the modularity matrix of a graph was defined as

$$M = A - \frac{dd^T}{2C}, \quad (13)$$

where  $A$  is the adjacency matrix,  $d = (d_1, \dots, d_n)^T$  is the *degree-vector* comprised of the vertices degrees and  $C = \frac{1}{2} \sum_{i=1}^n d_i$  is the total number of edges in the network.

### Laplacian and normalized Laplacian

Laplacian is widely used in spectral manifold learning methods, a framework known as Laplacian Eigenmaps. The graph Laplacian matrix is defined as

$$L = D - A, \quad (14)$$

where  $A$  is the adjacency and  $D$  is the diagonal matrix of degrees. Though Laplacian is related to many physical phenomena, such as heat propagation, a more direct connection with random walks is provided by the Normalized Laplacian (or Random Walks Laplacian),  $L_{RW} = D^{-1}L$ , which is also frequently used for clustering. Note that  $L_{RW}$  is non-symmetric, however, its spectrum is real. Obviously,  $L_{RW}$  has the same set of eigenvalues as the symmetric normalized Laplacian

$$L_{norm} = D^{1/2} L_{RW} D^{-1/2} = D^{-1/2} L D^{-1/2} = I - D^{-1/2} A D^{-1/2}. \quad (15)$$

### Similarity measures

In order to assess the similarity between different partitions and biological benchmarks we use the adjusted mutual information score (AMI), defined as follows. Suppose that we have a set  $S$  and two partitions of  $S$ :  $U$  and  $V$ , the elements of the partitions are called clusters. Let us denote the probability that some random object falls into a cluster  $U_i$  of  $U$  as  $P_U(i)$  which is equal to  $\frac{|U_i|}{|S|}$ . The entropy calculated for the partition  $U$  is equal to  $H(U) = -\sum_{i=1}^R P_U(i) \log P_U(i)$ . Using the introduced notation, we can express the mutual information for  $U$  and  $V$  as

$$MI(U, V) := \sum_{i=1}^R \sum_{j=1}^C P_{UV}(i, j) \log \frac{P_{UV}(i, j)}{P_U(i)P_V(j)}. \quad (16)$$

Importantly, this measure of similarity tends to be larger when the two partitions have a larger number of clusters even when we use the same number of elements for clustering. To avoid such biases one can use the adjusted mutual information which is defined as

$$AMI(U, V) := \frac{MI(U, V) - E\{MI(U, V)\}}{\max\{H(U), H(V)\} - E\{MI(U, V)\}}, \quad (17)$$

where  $E\{MI(U, V)\}$  is the expected value of the mutual information of  $V$  and  $U$ .

Therefore, AMI is 0 when the similarity is equal to its expected value under random permutation of the vertices between the groups and 1 for identical partitions.